

Renormalized quark masses using gradient flow

Matthew Black,^{1,2} Robert V. Harlander,³ Anna Hasenfratz,^{4,*} Antonio Rago,⁵ and Oliver Witzel^{2,†}

¹*School of Physics and Astronomy, University of Edinburgh, Edinburgh EH9 3JZ, UK*

²*Theoretische Physik 1, Center for Particle Physics Siegen, Naturwissenschaftlich-Technische Fakultät, Universität Siegen, 57068 Siegen, Germany*

³*Institute for Theoretical Particle Physics and Cosmology, RWTH Aachen University, 52056 Aachen, Germany*

⁴*Department of Physics, University of Colorado, Boulder, Colorado 80309, USA*

⁵*IMADA and Quantum Theory Center, University of Southern Denmark, Odense, Denmark*

(Dated: June 23, 2025)

We propose a new and simple method for determining the renormalized quark masses from lattice simulations. Renormalized quark masses are an important input to many phenomenological applications, including searching/modeling physics beyond the Standard Model. The non-perturbative renormalization is performed using gradient flow combined with the short-flow-time expansion that is improved by renormalization group (RG) running to match to the $\overline{\text{MS}}$ -scheme. RG running connects the lattice scale to higher energies thus improving the $\overline{\text{MS}}$ -scheme matching. Implementing the RG running perturbatively, we demonstrate this method works reliably at least up to the charm-quark mass and is not exhibiting any signs of the usual “window problem”. Using RBC/UKQCD’s (2+1)-flavor Shamir domain-wall fermion ensembles with Iwasaki gauge action, we find $m_s^{\overline{\text{MS}}}(\mu = 2 \text{ GeV}) = 90(3) \text{ MeV}$ and $m_c^{\overline{\text{MS}}}(\mu = 3 \text{ GeV}) = 975(10) \text{ MeV}$. These results predict the scale-independent ratio $m_c/m_s = 12.0(4)$. Generalization to other observables is possible, providing an efficient approach to determine non-perturbatively renormalized fermionic observables like form factors or bag parameters from lattice simulations.

Introduction — Theoretical predictions for Standard Model (SM) processes require that non-perturbative effects due to the strong force are accounted for. These are typically expressed in terms of decay constants, form factors, bag parameters, etc. An ab initio way to determine such non-perturbative quantities is the framework of lattice Quantum Chromodynamics (QCD) which allows us to improve the associated uncertainties systematically. Lattice quantities need to be renormalized and matched to a continuum scheme. This matching requires a renormalization scheme that can be implemented on the lattice as well as in perturbation theory (PT). Different methods are employed, each with distinct pros and cons: The Schrödinger Functional [1–4] scheme uses gauge-invariant correlation functions, but the boundary conditions make perturbative calculations challenging. The regularization-independent momentum subtraction (RI/MOM) schemes [5] break gauge invariance and have a “window problem” arising from the need to choose a matching scale μ that is large enough to control the perturbative expansion, $\mu \gg \Lambda_{\text{QCD}}$, but small enough to avoid large cutoff effects, $\mu \ll 1/a$. Position-space schemes renormalization [6, 7] use gauge invariant correlation functions, where source–sink separation has to satisfy $a \ll t \ll \Lambda_{\text{QCD}}^{-1}$, creating a window problem.

In this work we develop a new method to calculate non-perturbatively renormalized quark masses using lattice QCD simulations and match them to the $\overline{\text{MS}}$ -scheme [8–10] using the short-flow-time expansion (SFTX) [8, 11, 12]. The procedure combines lattice and perturbative gradient flow (GF) [11, 13–15], improved by renormalization group (RG) running to bridge the lattice

and continuum energy scales. Our approach is gauge invariant, numerically precise, avoids most of the window problems, and is straightforward to implement ¹.

We demonstrate our method by predicting renormalized strange- and charm-quark masses. Precise values for the quark masses are an important input to many phenomenological applications, helping us to explore potential physics beyond the SM. We extract the renormalized quark-mass values in the GF scheme from the two-point correlation functions of flowed and regular pseudo-scalar and axial-vector currents using the partially conserved axial-vector current (PCAC) relation. The lattice calculation is performed on a set of (2+1)-flavor gauge-field configurations, and we use tuned strange- and charm-quark masses in the valence sector. After extrapolating to the continuum limit, we match the resulting GF renormalized quantities to the $\overline{\text{MS}}$ -scheme by multiplying with the corresponding SFTX coefficients and taking the limit to zero flow time ($\tau \rightarrow 0$).

We aid this matching by RG running the flow-time from the low energy lattice scale to values where PT becomes reliable. Currently, this step is based on the perturbatively evaluated GF mass anomalous dimension [17], but we envision replacing this with a non-perturbative running in the future [18]. This RG running improves the $\tau \rightarrow 0$ limit, making it better controlled and more stable compared to the unimproved extrapolation.

¹ An alternative approach based on flowed vacuum expectation values has been recently presented in [16].

Notation and definitions — The gradient-flow equation for the gauge field reads

$$\partial_\tau B_\mu = D_\nu G_{\nu\mu}, \quad (1)$$

where the flowed gauge field is related to the regular gluon field by $B_\mu(\tau=0) = A_\mu$, and

$$G_{\mu\nu} = \partial_\mu B_\nu - \partial_\nu B_\mu + [B_\mu, B_\nu], \quad D_\mu = \partial_\mu + [B_\mu, \cdot].$$

The evolution of the quark fields is given on the gauge background:

$$\partial_\tau \chi = \Delta \chi, \quad \partial_\tau \bar{\chi} = \bar{\chi} \overleftarrow{\Delta}, \quad \Delta = D_\mu D_\mu. \quad (2)$$

The flow regularizes ultra-violet (UV) divergences in composite operators of flowed gauge fields. Composite operators which also involve flowed fermions are finite only after a multiplicative fermion wave function renormalization is taken into account, $\chi_R = Z_\chi^{1/2} \chi$ [15, 19]. The perturbative approach to the flow equations has been discussed in Refs. [11, 14, 15, 20].

On the lattice, the gradient flow is an invertible smoothing transformation. Its numerical evaluation on the gauge fields is straightforward [21]. Fermionic quantities are always expressed as expectation values of quark propagators, requiring the inversion of the Dirac operator on some source. While flowing both “ends” of the propagator is numerically challenging, flowing only one end is again straightforward [15]. In the following, we consider current correlators where only the sinks are flowed.

Specifically, we are interested in the ratio

$$R_{rs}(t; \tau) = - \frac{\langle A_0(t; \tau) P(t=0; \tau=0) \rangle_{rs}}{\langle P(t; \tau) P(t=0; \tau=0) \rangle_{rs}}, \quad (3)$$

where t denotes Euclidean time, $A_0^{rs}(t; \tau)$ and $P^{rs}(t; \tau)$ are the zero-momentum axial and pseudo-scalar charge operators of (flowed) quark fields with flavors r and s . In this paper, we only consider flavor-nonsinglet (connected) correlators. Since Z_χ as well as the divergences stemming from $P(t=0; \tau=0)$ cancel in the ratio, $R_{rs}(t; \tau)$ is UV-finite.

Both correlators in Eq. (3) couple to the same pseudo-scalar state of mass M_{PS} . Thus, at large source-sink separation and assuming a negligible footprint $\sqrt{8\tau}$ of the flow, the ground state dominates and the ratio $R_{rs}(t; \tau)$ is independent of t . We define

$$\bar{R}(\tau) = \lim_{t \rightarrow \infty} R(t; \tau) \quad \text{with} \quad \sqrt{8\tau} \ll t. \quad (4)$$

The renormalized PCAC relation (Ward identity) then implies [22]

$$\left(m_{\text{GF}}^{(r)}(\tau) + m_{\text{GF}}^{(s)}(\tau) \right) = M_{\text{PS}}^{(rs)} \bar{R}_{rs}(\tau), \quad (5)$$

where $m_{\text{GF}}^{(r,s)}(\tau)$ is the renormalized quark mass of flavor r or s at scale τ in the GF scheme, and $M_{\text{PS}}^{(rs)}$ is the pseudo-scalar mass in the channel.

Finally, we need to connect $m_{\text{GF}}^{(r,s)}(\tau)$ to the renormalized quark mass in the $\overline{\text{MS}}$ scheme at some energy scale μ . This matching can be performed in the SFTX

$$m_{\overline{\text{MS}}}(\mu) = \lim_{\tau \rightarrow 0} \zeta_{AP}^{-1}(\mu, \tau) m_{\text{GF}}(\tau), \quad (6)$$

where $\zeta_{AP}(\mu, \tau) = \zeta_A(\mu, \tau) \zeta_P^{-1}(\mu, \tau)$, and ζ_A, ζ_P are the SFTX matching coefficients of the axial-vector and the pseudo-scalar currents. They are known perturbatively to next-to-next-to-leading order (NNLO) level [23], and depend on τ and μ via $\alpha_s(\mu)$ and $\ln \tau/\tau_\mu$, where $\tau_\mu \sim 1/\mu^2$. For the strong coupling $\alpha_s(\mu)$ to be in the perturbative regime, we need to choose τ_μ sufficiently small. At the same time we require $\sqrt{8\tau} \gg a$ to minimize cut-off effects in the lattice calculation. We therefore improve the matching in Eq. (6) by running the energy scale from the lattice flow time τ to the perturbative τ_μ .

This running is governed by the RG equation in the GF scheme,

$$\tau \partial_\tau \mathcal{O}(\tau) = \gamma_{\mathcal{O}}^{\text{GF}} \mathcal{O}(\tau), \quad (7)$$

where, in our case, $\mathcal{O} \in \{A, P\}$. As shown in Refs. [20, 24], the perturbative flowed anomalous dimension can be expressed in terms of the matching coefficients as $\gamma_{\mathcal{O}}^{\text{GF}} = \tau(\partial_\tau \zeta_{\mathcal{O}}) \zeta_{\mathcal{O}}^{-1}$, and—under certain conditions—knowledge of $\zeta_{\mathcal{O}}$ to order α_s^n allows to obtain $\gamma_{\mathcal{O}}^{\text{GF}}$ to order α_s^{n+1} . Integrating Eq. (7) leads to

$$m_{\overline{\text{MS}}}(\mu) = \lim_{\tau \rightarrow 0} \zeta_{AP}^{-1}(\mu, \tau_\mu) \times \exp \left(- \int_{\tau_\mu}^{\tau} d\tau' \frac{\gamma_m^{\text{GF}}(\tau')}{\tau'} \right) m_{\text{GF}}(\tau), \quad (8)$$

where it follows from the previous discussion that $\gamma_m^{\text{GF}} = \gamma_A^{\text{GF}} - \gamma_P^{\text{GF}}$. Choosing $\mu \gtrsim 2 \text{ GeV}$ and $\tau_\mu = e^{-\gamma_E}/(2\mu^2)$ [25], we find that $\zeta_{AP}(\mu, \tau_\mu)$ shows fast convergence, while the exponential factor partly resums the higher-order logarithms.

Ideally, the non-perturbative expression for $\gamma_m^{\text{GF}}(\tau)$ should be used in Eq. (8) and a way to obtain it is demonstrated in Refs. [18, 26, 27]. For two-flavor QCD γ_m^{GF} was found to be close to the perturbative prediction [18]. Since we do not have non-perturbative values for γ_m^{GF} at $N_f = 2 + 1$, we use the perturbative expression known to α_s^3 [23].

The energy scale μ in Eq. (8) is arbitrary. We can evaluate $m_{\overline{\text{MS}}}$ at some different scale μ_{UV} and convert the result to the desired μ value by four-loop running in the $\overline{\text{MS}}$ scheme.² Although the final result should be independent of the choice of such an intermediate scale, the $\tau \rightarrow 0$ extrapolation in Eqs. (6) and (8) might not be. Any dependence on μ_{UV} could therefore be considered as a systematic uncertainty.

² This assumes $\alpha_s(\mu)$ and $\alpha_s(\mu_{\text{UV}})$ are small such that the perturbative series converges.

Numerical setup, analysis and results — We determine the strange and charm quark masses m_s and m_c , and obtain their ratio m_c/m_s using RBC/UKQCD’s set of (2+1)-flavor Shamir domain-wall fermion (DWF) and Iwasaki gauge field ensembles [28–32]. These ensembles feature three different bare gauge couplings, corresponding to inverse lattice spacings a^{-1} ranging from 1.78 to 2.78 GeV, as well as different unitary pion masses (due to different light sea-quark masses). Details of the ensembles are provided in Table S-I.³ Bare physical strange-quark masses and inverse lattice spacings are taken from Refs. [30, 32], and bare physical charm-quark masses are tuned using the D_s meson. Our lattice calculations are based on Grid [34] and Hadrons [35, 36], and we implemented fermionic gradient flow [9, 10, 37] in Hadrons.⁴

We calculate the correlation functions of Eq. (3) at $\tau = 0$ by placing Z_2 wall sources [38, 39] on several time slices per configuration and individually invert the Dirac operator to obtain quark propagators. For the strange quark, we apply Gaussian source smearing [40] before inverting Shamir DWF [41–43], whereas for the charm quark we directly invert stout-smearred Möbius DWF [44–46]. Our calculation proceeds by evolving the gauge-field configuration together with the strange- and charm-quark propagators with GF as specified by Eqs. (1) and (2). We choose a step size $\epsilon = 0.01$ for the GF evolution and contract the quark propagators imposing a point sink every 10th (for larger flow times every 40th) step to obtain the corresponding two-point correlators as functions of the GF time τ . Sources and sinks are projected to zero momentum.

We average correlators calculated with different source positions on the same gauge field and afterwards use jack-knife resampling to propagate statistical uncertainties. We extract the pseudo-scalar meson mass M_{PS} and verify that it is indeed independent of flow time τ . The corresponding values are listed in Table S-II. Next we extract $R(t/a; \tau/a^2)$ as defined in Eq. (3) for a range of lattice flow times $0 \leq \tau/a^2 \leq 8$.

As an example, we show the resulting correlator ratios for the D_s meson on the F1S ensemble for a selection of GF times in Fig. S-1. Values for $\bar{R}(\tau/a^2)$ are extracted by performing correlated fits to the plateaus. After repeating this step for all six ensembles, we show \bar{R} as a function of the lattice flow time τ/a^2 in the upper panel of Fig. 1. Next, we multiply our ratios with the corresponding lattice value of $aM_{PS}/2$ and convert both aM_{PS} and the lattice flow time τ/a^2 to physical units using the inverse lattice spacings listed in Table S-I. The result is

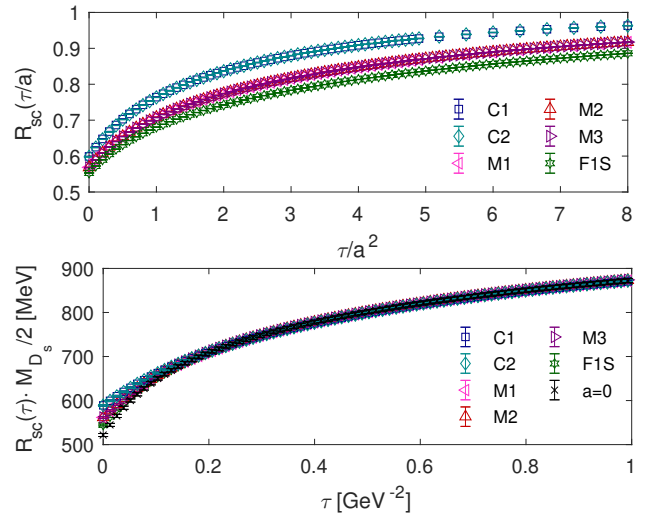


FIG. 1. Extracting \bar{R} -ratios (see Eq. (4)) for D_s meson correlators. Top: dependence on the flow time τ/a in lattice units for our six ensembles. Bottom: converting to physical units and adding the $a \rightarrow 0$ continuum limit predictions.

shown in the lower panel of Fig. 1. In the upper panel, data corresponding to the different coarse and medium ensembles sit on top of each other, indicating that sea-quark effects are not resolved in the \bar{R} ratios. In the lower panel, the six ratios form a unique curve, showing deviation due to cut-off effects only in the small- τ region. We interpolate the flow times in the coarse and medium ensembles to match the values on the F1S ensemble and take the continuum limit $a \rightarrow 0$ for the different flow times τ . Since all actions used in this calculation are $\mathcal{O}(a)$ -improved and no sea-quark effects are resolved, we simply perform a linear extrapolation in a^2 to arrive at the continuum-limit results shown by the black crosses in the lower panel of Fig. 1.

The continuum limit results for $m_{GF}(\tau)$ are renormalized in the GF-scheme. We have to take the $\tau \rightarrow 0$ limit to connect to the mass-independent \overline{MS} scheme following Eq. (6). We can improve the matching using RG running according to Eq. (8). To validate the consistency of our results, we use γ_m^{GF} at order α_s^2 for the next-to-leading order (NLO) improvement, and at order α_s^3 for the NNLO improvement. The larger right panel of Fig. 2 shows $\zeta_{AP}^{-1}(\tau, \mu)m_{GF}(\tau)$ and the corresponding RG improved values for the D_s system as a function of the flow time τ both at NLO and NNLO level. We use $N_f = 4$ for the $\zeta_{AP}(\tau, \mu)$ factor and the RG running.

At small flow time $\sqrt{8\tau} \lesssim a$, the lattice data are contaminated by lattice artifacts. On the coarsest ensembles, this corresponds to $\tau < 0.039 \text{ GeV}^{-2}$. To obtain the $\tau \rightarrow 0$ limit we consider two fit ansätze:⁵

³ References with a prefixed “S-” refer to tables and figures in the Supplemental Material [33].

⁴ Cf. <https://github.com/aportelli/Hadrons/pull/137> and examples given at <https://github.com/mbr-phys/HeavyMesonLifetimes>.

⁵ Alternative approaches are discussed in [47].

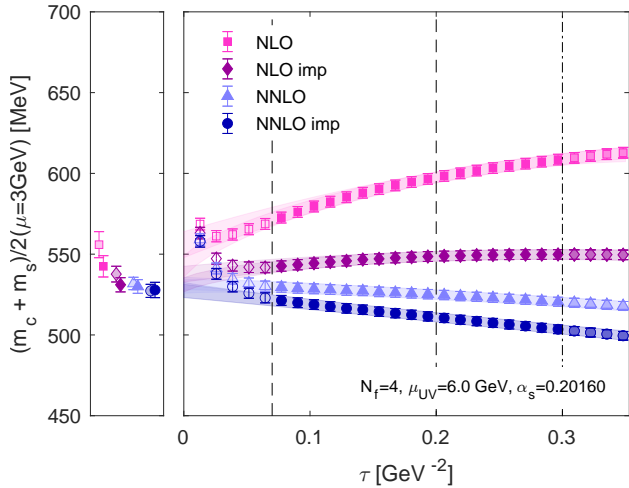


FIG. 2. The large panel illustrates extracting $(m_c + m_s)/2$ at the renormalization scale $\mu_{UV} = 6$ GeV, converted to $\mu = 3$ GeV using 4-loop $N_f = 4$ $\overline{\text{MS}}$ running. Pink squares and light blue triangles denote to the NLO and the NNLO values, respectively. Purple diamonds and dark blue circles show the corresponding RG improved NLO and NNLO values. The $\tau \rightarrow 0$ limit is taken in a $(\tau_{\min}, \tau_{\max})$ range as explained in the text. The shaded error bands show the maximal spread of quadratic or linear-log fits using the central values plus/minus their uncertainty. Only filled symbols enter the $\tau \rightarrow 0$ extrapolation. The small panel compares the final predictions using solid filled symbols for linear-log and shaded fillings for quadratic fits.

quadratic $f_2(\tau) = \tau^2 c_2 + c_1 + c_0$ and linear-log $f_l(\tau) = \tau(c_l \log(\tau\mu^2) + c_1) + c_0$. Moreover, we vary the fit range and always account for the maximal variation using $\tau_{\min} \in (0.078, 0.2)$ GeV $^{-2}$ with $\tau_{\max} = 0.3$ GeV $^{-2}$, and $\tau_{\max} \in (0.25, 0.35)$ GeV $^{-2}$ with $\tau_{\min} = 0.14$ GeV $^{-2}$ to obtain the color-shaded bands in Fig. 2. Since successive data in GF time tend to be highly correlated, we take the limit $\tau \rightarrow 0$ by performing uncorrelated fits to the central values plus/minus their uncertainties. For better visibility, we show the two final fit values for the four different approximations (NLO, NNLO, with and without RG improvement) in the left panel of Fig. 2. While there is only very little difference for the NNLO results with and without RG running, the NLO result improves substantially. The overall approach to zero becomes flatter, and the spread between our different fit ansätze reduces. In Fig. 3 we show the dependence on the μ_{UV} scale. The NNLO RG improved results show very little variation in the $3 \text{ GeV} < \mu_{UV} < 12 \text{ GeV}$ range, and even the NLO predictions are consistent for $3 \text{ GeV} < \mu_{UV} \lesssim 6 \text{ GeV}$. For our final result we quote the full spread of all fits to the NNLO improved data

$$\frac{m_c + m_s}{2} = 528(5) \text{ MeV} \quad \text{at } \mu = 3 \text{ GeV}, \quad (9)$$

where the uncertainty covers both statistical and systematic effects. The $\tau \rightarrow 0$ and $a \rightarrow 0$ extrapolations dom-

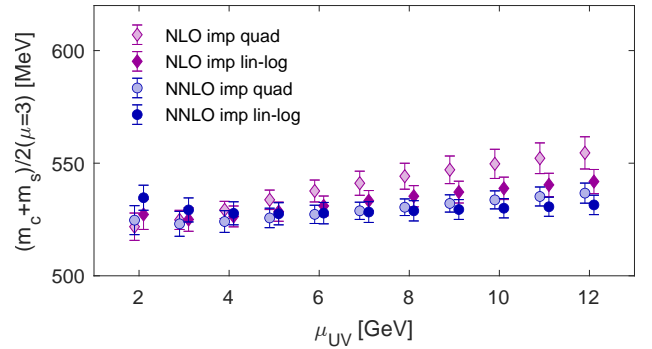


FIG. 3. Dependence of $(m_c + m_s)/2$ obtained from D_s correlators on μ_{UV} .

inate the systematic effects. As part of our analysis, we have included the uncertainty of a^{-1} and the tuning of the bare charm mass, whereas effects due to choosing the fit range to obtain $\bar{R}(\tau/a)$ or finite volume effects are negligible.

Repeating the steps outlined above, we analyze data that describe the charmonium state η_c as well as the (unphysical) $(s\bar{s})$ -bound state, which we refer to as η_s . Details for η_c are presented in Fig. S-2 where we prefer a larger value of $\mu_{UV} = 8$ GeV. In the case of η_s , we observe a tension in M_{η_s} on the F1S ensemble w.r.t. our determinations on the coarse and medium ensembles (cf. Table S-II) which we attribute to a slight misdetermination of the bare strange quark mass. Hence we discard the F1S data for this analysis and show our final result based on data from the medium and coarse ensembles in Fig. S-3. Since with only two lattice spacings a linear ansatz for the $a \rightarrow 0$ limit is poorly constrained, we consider in addition fitting a constant. Both $a \rightarrow 0$ extrapolations have good p -values, so we take the spread when obtaining the value of m_s , essentially doubling its error. We find

$$m_c^{\eta_c}(\mu = 3 \text{ GeV}) = 1006(25) \text{ MeV} \quad (10)$$

$$m_s(\mu = 2 \text{ GeV}) = 90(3) \text{ MeV}. \quad (11)$$

Combining our result in Eq. (9) with the value for m_s of Eq. (11), run up to $\mu = 3$ GeV, we obtain the more precise value

$$m_c(\mu = 3 \text{ GeV}) = 975(10) \text{ MeV}, \quad (12)$$

which we also utilize to deduce the ratio

$$\frac{m_c}{m_s} = 12.0(4). \quad (13)$$

A comparison of our values for the strange and charm quark mass to the literature is shown in Fig. 4.

Summary — Gradient-flowed quark propagators provide a simple, non-perturbative method to renormalize fermionic quantities. Matching to the perturbative $\overline{\text{MS}}$ scheme can be performed using SFTX. Using RG running, the convergence can be further improved, avoiding

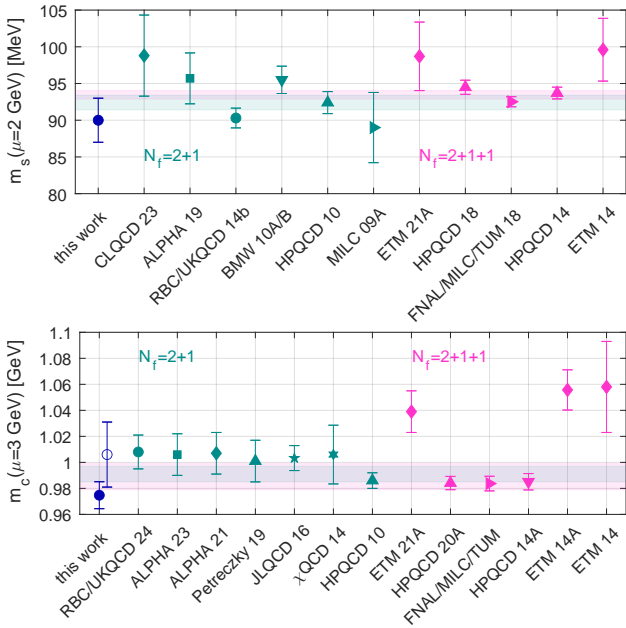


FIG. 4. Comparison of our strange and charm quark masses (blue circles) to the FLAG averages [48] (shaded bands) for 2+1 and 2+1+1 flavors. We show the direct prediction for m_c with open circle, and the determination from the D_s meson with filled circle. Also shown are results entering FLAG averages: strange 2+1 [49–55], strange 2+1+1 [56–60], charm 2+1 [52, 61–65], charm 2+1+1 [56, 58–60, 66, 67], as well as a new result not part of the average [68].

the window problem. We implement and test this idea to obtain renormalized strange and charm quark masses at percent-level accuracy. The accuracy can easily be improved by using state-of-the-art physical point gauge field configurations and finer lattice spacings. The GF is a mass-dependent renormalization scheme and the matching to the mass-independent $\overline{\text{MS}}$ scheme requires taking the $\tau \rightarrow 0$ limit. The RG running is important to improve the convergence. Determining $\gamma_m^{\text{GF}}(\tau)$ of Eq. (8) non-perturbatively is an interesting task for the future.

Since the GF directly renormalizes the fermionic operator, also “mixed action” setups using different fermion discretizations for light and heavy quarks (as we do for the D_s meson) can be non-perturbatively renormalized. PT only enters when matching to the continuum $\overline{\text{MS}}$ scheme using SFTX.

Acknowledgment — We thank the RBC/UKQCD Collaboration for generating and making their gauge field ensembles publicly available. The data analyzed here were generated as part of the project to calculate heavy meson lifetimes [37].

We thank Jonas Kohnen, Fabian Lange, Christopher Monahan, Matthew Rizik, Andrea Shindler, Rainer Sommer, and Tobias Tsang for fruitful discussions. A.H. and O.W. are grateful for the hospitality at the Kavli Institute of Theoretical Physics at UC Santa Barbara, where

part of this work was carried out during the program “What is Particle Theory?”. A.H. thanks the University of Siegen for the hospitality she received during the final stages of this work.

These computations used resources provided by the OMNI cluster at the University of Siegen, the HAWK cluster at the High-Performance Computing Center Stuttgart, and LUMI-G at the CSC data center Finland (DeiC National HPC g.a. DEIC-SDU-L5-13 and DEIC-SDU-N5-2024053).

M.B., R.H., O.W. received support from the Deutsche Forschungsgemeinschaft (DFG, German Research Foundation) through grant 396021762 — TRR 257 “Particle Physics Phenomenology after the Higgs Discovery”. M.B. was additionally funded in part by UK STFC grant ST/X000494/1. A.H. acknowledges support from DOE grant DE-SC001000. This research was supported in part by grant NSF PHY-2309135 to the Kavli Institute for Theoretical Physics (KITP).

Data availability — The c++ lattice QCD software libraries `Grid` [34] and `Hadrons` [35, 36] are open source and publicly available. Matthew Black implemented fermionic gradient flow [9, 10, 37] in `Hadrons`: <https://github.com/aportelli/Hadrons/pull/137> with examples given at <https://github.com/mbr-phys/HeavyMesonLifetimes>. Data for the two-point correlation functions used in this project will be made available as part of the data release for Ref. [37].

* Contact author: anna.hasenfratz@colorado.edu

† Contact author: oliver.witzel@uni-siegen.de

- [1] M. Lüscher, R. Narayanan, P. Weisz, and U. Wolff, The Schrödinger functional: A Renormalizable probe for non-Abelian gauge theories, *Nucl. Phys. B* **384**, 168 (1992), [arXiv:hep-lat/9207009](https://arxiv.org/abs/hep-lat/9207009).
- [2] M. Lüscher, R. Sommer, P. Weisz, and U. Wolff, A Precise determination of the running coupling in the SU(3) Yang-Mills theory, *Nucl. Phys. B* **413**, 481 (1994), [arXiv:hep-lat/9309005](https://arxiv.org/abs/hep-lat/9309005).
- [3] S. Sint, On the Schrödinger functional in QCD, *Nucl. Phys. B* **421**, 135 (1994), [arXiv:hep-lat/9312079](https://arxiv.org/abs/hep-lat/9312079).
- [4] S. Capitani, M. Lüscher, R. Sommer, and H. Wittig, Non-perturbative quark mass renormalization in quenched lattice QCD, *Nucl. Phys. B* **544**, 669 (1999), [Erratum: *Nucl.Phys.B* 582, 762–762 (2000)], [arXiv:hep-lat/9810063](https://arxiv.org/abs/hep-lat/9810063).
- [5] G. Martinelli, C. Pittori, C. T. Sachrajda, M. Testa, and A. Vladikas, A General method for nonperturbative renormalization of lattice operators, *Nucl. Phys. B* **445**, 81 (1995), [arXiv:hep-lat/9411010](https://arxiv.org/abs/hep-lat/9411010).
- [6] G. Martinelli, G. C. Rossi, C. T. Sachrajda, S. R. Sharpe, M. Talevi, and M. Testa, Nonperturbative improvement of composite operators with Wilson fermions, *Phys. Lett. B* **411**, 141 (1997), [arXiv:hep-lat/9705018](https://arxiv.org/abs/hep-lat/9705018).
- [7] V. Gimenez, L. Giusti, S. Guerriero, V. Lubicz, G. Martinelli, S. Petrarca, J. Reyes, B. Taglienti, and E. Trevisani,

- gine, Non-perturbative renormalization of lattice operators in coordinate space, *Phys. Lett. B* **598**, 227 (2004), [arXiv:hep-lat/0406019](#).
- [8] H. Suzuki, Energy–momentum tensor from the Yang–Mills gradient flow, *PTEP* **2013**, 083B03 (2013), [Erratum: PTEP 2015, 079201 (2015)], [arXiv:1304.0533 \[hep-lat\]](#).
- [9] M. Black, R. Harlander, F. Lange, A. Rago, A. Shindler, and O. Witzel, Using Gradient Flow to Renormalise Matrix Elements for Meson Mixing and Lifetimes, *PoS LATTICE2023*, 263 (2024), [arXiv:2310.18059 \[hep-lat\]](#).
- [10] M. Black, R. Harlander, F. Lange, A. Rago, A. Shindler, and O. Witzel, Gradient Flow Renormalisation for Meson Mixing and Lifetimes, *PoS LATTICE2024*, 243 (2025), [arXiv:2409.18891 \[hep-lat\]](#).
- [11] M. Lüscher and P. Weisz, Perturbative analysis of the gradient flow in non-abelian gauge theories, *JHEP* **1102**, 051, [arXiv:1101.0963 \[hep-th\]](#).
- [12] M. Lüscher, Future applications of the Yang-Mills gradient flow in lattice QCD, *PoS LATTICE2013*, 016 (2014), [arXiv:1308.5598 \[hep-lat\]](#).
- [13] R. Narayanan and H. Neuberger, Infinite N phase transitions in continuum Wilson loop operators, *JHEP* **0603**, 064, [arXiv:hep-th/0601210 \[hep-th\]](#).
- [14] M. Lüscher, Properties and uses of the Wilson flow in lattice QCD, *JHEP* **1008**, 071, [arXiv:1006.4518 \[hep-lat\]](#).
- [15] M. Lüscher, Chiral symmetry and the Yang–Mills gradient flow, *JHEP* **1304**, 123, [arXiv:1302.5246 \[hep-lat\]](#).
- [16] H. Takaura, R. V. Harlander, and F. Lange, A new approach to quark mass determination using the gradient flow, (2025), [arXiv:2506.09537 \[hep-lat\]](#).
- [17] R. V. Harlander, F. Lange, and T. Neumann, Hadronic vacuum polarization using gradient flow, *JHEP* **08**, 109, [arXiv:2007.01057 \[hep-lat\]](#).
- [18] A. Hasenfratz, C. J. Monahan, M. D. Rizik, A. Shindler, and O. Witzel, A novel nonperturbative renormalization scheme for local operators, *PoS LATTICE2021*, 155 (2022), [arXiv:2201.09740 \[hep-lat\]](#).
- [19] A. Carosso, A. Hasenfratz, and E. T. Neil, Nonperturbative Renormalization of Operators in Near-Conformal Systems Using Gradient Flows, *Phys. Rev. Lett.* **121**, 201601 (2018), [arXiv:1806.01385 \[hep-lat\]](#).
- [20] J. Artz, R. V. Harlander, F. Lange, T. Neumann, and M. Prausa, Results and techniques for higher order calculations within the gradient-flow formalism, *JHEP* **06**, 121, [erratum: JHEP10,032(2019)], [arXiv:1905.00882 \[hep-lat\]](#).
- [21] M. Lüscher, Trivializing maps, the Wilson flow and the HMC algorithm, *Commun. Math. Phys.* **293**, 899 (2010), [arXiv:0907.5491 \[hep-lat\]](#).
- [22] T. Endo, K. Hieda, D. Miura, and H. Suzuki, Universal formula for the flavor non-singlet axial-vector current from the gradient flow, *PTEP* **2015**, 053B03 (2015), [arXiv:1502.01809 \[hep-lat\]](#).
- [23] J. Borgulat, R. V. Harlander, J. T. Kohnen, and F. Lange, Short-flow-time expansion of quark bilinears through next-to-next-to-leading order QCD, *JHEP* **05**, 179, [arXiv:2311.16799 \[hep-lat\]](#).
- [24] J. Borgulat, N. Felten, R. Harlander, and J. T. Kohnen, Two-loop gradient-flow renormalization of scalar QCD, *SciPost Phys. Core* **8**, 032 (2025), [arXiv:2501.07150 \[hep-ph\]](#).
- [25] R. V. Harlander, Y. Kluth, and F. Lange, The two-loop energy–momentum tensor within the gradient-flow formalism, *Eur. Phys. J. C* **78**, 944 (2018), [Erratum: Eur. Phys. J.C79,no.10,858(2019)], [arXiv:1808.09837 \[hep-lat\]](#).
- [26] A. Hasenfratz, E. T. Neil, Y. Shamir, B. Svetitsky, and O. Witzel, Infrared fixed point and anomalous dimensions in a composite Higgs model, *Phys. Rev. D* **107**, 114504 (2023), [arXiv:2304.11729 \[hep-lat\]](#).
- [27] A. Hasenfratz, E. T. Neil, Y. Shamir, B. Svetitsky, and O. Witzel, Infrared fixed point of the SU(3) gauge theory with Nf=10 flavors, *Phys. Rev. D* **108**, L071503 (2023), [arXiv:2306.07236 \[hep-lat\]](#).
- [28] C. Allton *et al.* (RBC/UKQCD), Physical Results from 2+1 Flavor Domain Wall QCD and SU(2) Chiral Perturbation Theory, *Phys. Rev. D* **78**, 114509 (2008), [arXiv:0804.0473 \[hep-lat\]](#).
- [29] Y. Aoki *et al.* (RBC/UKQCD), Continuum Limit Physics from 2+1 Flavor Domain Wall QCD, *Phys.Rev. D* **83**, 074508 (2011), [arXiv:1011.0892 \[hep-lat\]](#).
- [30] T. Blum *et al.* (RBC/UKQCD), Domain wall QCD with physical quark masses, *Phys. Rev. D* **93**, 074505 (2016), [arXiv:1411.7017 \[hep-lat\]](#).
- [31] P. A. Boyle *et al.* (RBC/UKQCD), The decay constants f_D and f_{D_s} in the continuum limit of $N_f = 2 + 1$ domain wall lattice QCD, *JHEP* **12**, 008, [arXiv:1701.02644 \[hep-lat\]](#).
- [32] P. A. Boyle *et al.* (RBC/UKQCD), SU(3)-breaking ratios for $D_{(s)}$ and $B_{(s)}$ mesons, (2018), [arXiv:1812.08791 \[hep-lat\]](#).
- [33] See supplemental material.
- [34] P. Boyle, A. Yamaguchi, G. Cossu, and A. Portelli, Grid: A next generation data parallel C++ QCD library, *PoS LATTICE2015*, 023 (2016), [arXiv:1512.03487 \[hep-lat\]](#).
- [35] A. Portelli *et al.*, *Hadrons*.
- [36] A. Portelli *et al.*, [github.com/aportelli/hadrons: Hadrons v1.3](#) (2022).
- [37] M. Black, R. Harlander, J. Kohnen, F. Lange, A. Rago, A. Shindler, and O. Witzel, Lattice determination of heavy meson lifetimes (2025), (in preparation).
- [38] C. McNeile and C. Michael (UKQCD), Decay width of light quark hybrid meson from the lattice, *Phys. Rev. D* **73**, 074506 (2006), [arXiv:hep-lat/0603007](#).
- [39] P. A. Boyle, A. Jüttner, C. Kelly, and R. D. Kenway, Use of stochastic sources for the lattice determination of light quark physics, *JHEP* **08**, 086, [arXiv:0804.1501 \[hep-lat\]](#).
- [40] S. Güsken, U. Löw, K. H. Mütter, R. Sommer, A. Patel, and K. Schilling, Nonsinglet Axial Vector Couplings of the Baryon Octet in Lattice QCD, *Phys. Lett. B* **227**, 266 (1989).
- [41] D. B. Kaplan, A Method for simulating chiral fermions on the lattice, *Phys. Lett. B* **288**, 342 (1992), [arXiv:hep-lat/9206013](#).
- [42] Y. Shamir, Chiral fermions from lattice boundaries, *Nucl. Phys. B* **406**, 90 (1993), [arXiv:hep-lat/9303005](#).
- [43] V. Furman and Y. Shamir, Axial symmetries in lattice QCD with Kaplan fermions, *Nucl. Phys. B* **439**, 54 (1995), [arXiv:hep-lat/9405004](#).
- [44] C. Morningstar and M. J. Peardon, Analytic smearing of SU(3) link variables in lattice QCD, *Phys. Rev. D* **69**, 054501 (2004), [arXiv:hep-lat/0311018](#).
- [45] R. C. Brower, H. Neff, and K. Orginos, The Möbius domain wall fermion algorithm, *Comput. Phys. Commun.* **220**, 1 (2017), [arXiv:1206.5214 \[hep-lat\]](#).
- [46] Y.-G. Cho, S. Hashimoto, A. Jüttner, T. Kaneko, M. Marinkovic, J.-I. Noaki, and J. T. Tsang, Improved

- lattice fermion action for heavy quarks, *JHEP* **05**, 072, [arXiv:1504.01630 \[hep-lat\]](#).
- [47] H. Suzuki and H. Takaura, $t \rightarrow 0$ extrapolation function in the small flow time expansion method for the energy-momentum tensor, *PTEP* **2021**, 073B02 (2021), [arXiv:2102.02174 \[hep-lat\]](#).
- [48] Y. Aoki *et al.* (Flavour Lattice Averaging Group (FLAG)), FLAG Review 2024, (2024), [arXiv:2411.04268 \[hep-lat\]](#).
- [49] Z.-C. Hu *et al.* (CLQCD), Quark masses and low-energy constants in the continuum from the tadpole-improved clover ensembles, *Phys. Rev. D* **109**, 054507 (2024), [arXiv:2310.00814 \[hep-lat\]](#).
- [50] M. Bruno, I. Campos, P. Fritzscht, J. Koponen, C. Pena, D. Preti, A. Ramos, and A. Vladikas (ALPHA), Light quark masses in $N_f = 2 + 1$ lattice QCD with Wilson fermions, *Eur. Phys. J. C* **80**, 169 (2020), [arXiv:1911.08025 \[hep-lat\]](#).
- [51] T. Blum *et al.* (RBC, UKQCD), Domain wall QCD with physical quark masses, *Phys. Rev. D* **93**, 074505 (2016), [arXiv:1411.7017 \[hep-lat\]](#).
- [52] C. McNeile, C. T. H. Davies, E. Follana, K. Hornbostel, and G. P. Lepage, High-Precision c and b Masses, and QCD Coupling from Current-Current Correlators in Lattice and Continuum QCD, *Phys. Rev. D* **82**, 034512 (2010), [arXiv:1004.4285 \[hep-lat\]](#).
- [53] S. Dürr, Z. Fodor, C. Hoelbling, S. D. Katz, S. Krieg, T. Kurth, L. Lellouch, T. Lippert, K. K. Szabo, and G. Vulvert (BMW), Lattice QCD at the physical point: light quark masses, *Phys. Lett. B* **701**, 265 (2011), [arXiv:1011.2403 \[hep-lat\]](#).
- [54] S. Dürr, Z. Fodor, C. Hoelbling, S. D. Katz, S. Krieg, T. Kurth, L. Lellouch, T. Lippert, K. K. Szabo, and G. Vulvert (BMW), Lattice QCD at the physical point: Simulation and analysis details, *JHEP* **08**, 148, [arXiv:1011.2711 \[hep-lat\]](#).
- [55] A. Bazavov *et al.* (MILC), MILC results for light pseudoscalars, *PoS CD09*, 007 (2009), [arXiv:0910.2966 \[hep-ph\]](#).
- [56] C. Alexandrou *et al.* (Extended Twisted Mass), Quark masses using twisted-mass fermion gauge ensembles, *Phys. Rev. D* **104**, 074515 (2021), [arXiv:2104.13408 \[hep-lat\]](#).
- [57] A. T. Lytle, C. T. H. Davies, D. Hatton, G. P. Lepage, and C. Sturm (HPQCD), Determination of quark masses from $n_f = 4$ lattice QCD and the RI-SMOM intermediate scheme, *Phys. Rev. D* **98**, 014513 (2018), [arXiv:1805.06225 \[hep-lat\]](#).
- [58] A. Bazavov *et al.* (Fermilab Lattice, MILC, TUMQCD), Up-, down-, strange-, charm-, and bottom-quark masses from four-flavor lattice QCD, *Phys. Rev. D* **98**, 054517 (2018), [arXiv:1802.04248 \[hep-lat\]](#).
- [59] B. Chakraborty, C. T. H. Davies, B. Galloway, P. Knecht, J. Koponen, G. C. Donald, R. J. Dowdall, G. P. Lepage, and C. McNeile, High-precision quark masses and QCD coupling from $n_f = 4$ lattice QCD, *Phys. Rev. D* **91**, 054508 (2015), [arXiv:1408.4169 \[hep-lat\]](#).
- [60] N. Carrasco *et al.* (European Twisted Mass), Up, down, strange and charm quark masses with $N_f = 2+1+1$ twisted mass lattice QCD, *Nucl. Phys. B* **887**, 19 (2014), [arXiv:1403.4504 \[hep-lat\]](#).
- [61] A. Bussone, A. Conigli, J. Frison, G. Herdoíza, C. Pena, D. Preti, A. Sáez, and J. Ugarrio (Alpha), Hadronic physics from a Wilson fermion mixed-action approach: charm quark mass and $D_{(s)}$ meson decay constants, *Eur. Phys. J. C* **84**, 506 (2024), [arXiv:2309.14154 \[hep-lat\]](#).
- [62] J. Heitger, F. Joswig, and S. Kuberski (ALPHA), Determination of the charm quark mass in lattice QCD with $2 + 1$ flavours on fine lattices, *JHEP* **05**, 288, [arXiv:2101.02694 \[hep-lat\]](#).
- [63] P. Petreczky and J. H. Weber, Strong coupling constant and heavy quark masses in $(2+1)$ -flavor QCD, *Phys. Rev. D* **100**, 034519 (2019), [arXiv:1901.06424 \[hep-lat\]](#).
- [64] K. Nakayama, B. Fahy, and S. Hashimoto, Short-distance charmonium correlator on the lattice with Möbius domain-wall fermion and a determination of charm quark mass, *Phys. Rev. D* **94**, 054507 (2016), [arXiv:1606.01002 \[hep-lat\]](#).
- [65] Y.-B. Yang *et al.*, Charm and strange quark masses and f_{D_s} from overlap fermions, *Phys. Rev. D* **92**, 034517 (2015), [arXiv:1410.3343 \[hep-lat\]](#).
- [66] D. Hatton, C. T. H. Davies, B. Galloway, J. Koponen, G. P. Lepage, and A. T. Lytle (HPQCD), Charmonium properties from lattice QCD+QED: Hyperfine splitting, J/ψ leptonic width, charm quark mass, and a_μ^c , *Phys. Rev. D* **102**, 054511 (2020), [arXiv:2005.01845 \[hep-lat\]](#).
- [67] C. Alexandrou, V. Drach, K. Jansen, C. Kallidonis, and G. Koutsou, Baryon spectrum with $N_f = 2 + 1 + 1$ twisted mass fermions, *Phys. Rev. D* **90**, 074501 (2014), [arXiv:1406.4310 \[hep-lat\]](#).
- [68] L. Del Debbio, F. Erben, J. M. Flynn, R. Mukherjee, and J. T. Tsang (RBC, UKQCD), Absorbing discretization effects with a massive renormalization scheme: The charm-quark mass, *Phys. Rev. D* **110**, 054512 (2024), [arXiv:2407.18700 \[hep-lat\]](#).

SUPPLEMENTAL MATERIAL: RENORMALIZED QUARK MASSES USING GRADIENT FLOW

TABLE S-I. RBC/UKQCD's $N_f = 2 + 1$ Shamir DWF ensembles with Iwasaki gauge action [28–32] specified by the inverse lattice spacing (a^{-1}), unitary pion mass (M_π), valence strange (am_s^{val}) and charm (am_c) quark masses. For the coarse (C1, C2), medium (M1, M2, M3) and fine ensemble (F1S) we use N_{conf} number of configurations and place N_{src} Z_2 wall-sources per configuration.

	L/a	T/a	a^{-1} [GeV]	M_π [MeV]	am_s^{val}	am_c	$N_{\text{src}} \times N_{\text{conf}}$
C1	24	64	1.7848(50)	340	0.03224	0.64	32×101
C2	24	64	1.7848(50)	433	0.03224	0.64	32×101
M1	32	64	2.3833(86)	302	0.02477	0.45	32×79
M2	32	64	2.3833(86)	362	0.02477	0.45	32×89
M3	32	64	2.3833(86)	411	0.02477	0.45	32×68
F1S	48	96	2.785(11)	267	0.02167	0.37	24×98

TABLE S-II. Values of the pseudo-scalar meson masses M_{η_s} , M_{D_s} , and M_{η_c} obtained for our six ensembles. First we list each mass in lattice units with statistical uncertainty only. Next we convert the value to MeV using a^{-1} quoted in Table S-I and the statistical uncertainty as well as the uncertainty propagated from a^{-1} .

	aM_{η_s}	M_{η_s} [MeV]	aM_{D_s}	M_{D_s} [MeV]	aM_{η_c}	M_{η_c} [MeV]
C1	0.38961(51)	695.38(0.9)(1.9)	1.10198(66)	1966.8(1.2)(5.5)	1.64713(21)	2939.81(0.4)(8.2)
C2	0.39204(44)	699.71(0.8)(2.0)	1.10408(63)	1970.6(1.1)(5.5)	1.64812(17)	2941.57(0.3)(8.2)
M1	0.29175(35)	695.33(0.8)(2.5)	0.82889(48)	1975.5(1.1)(7.1)	1.24895(16)	2976.61(0.4)(10.7)
M2	0.29214(41)	696.26(1.0)(2.5)	0.82933(49)	1976.5(1.2)(7.1)	1.24923(16)	2977.28(0.4)(10.7)
M3	0.29281(36)	697.86(0.9)(2.5)	0.82995(57)	1978.0(1.4)(7.1)	1.24964(20)	2978.26(0.5)(10.7)
F1S	0.25512(19)	710.50(0.5)(2.8)	0.70717(37)	1969.5(1.0)(7.8)	1.065287(87)	2966.82(0.2)(11.7)

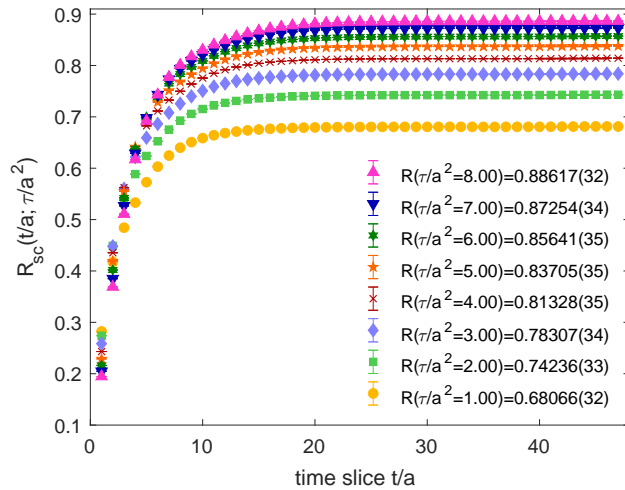


FIG. S-1. Ratios $R(t/a; \tau/a^2)$ defined in Eq. (3) for selected flow times τ/a^2 for the D_s meson on the F1S ensemble. Statistical errors are within the symbol sizes.

Due to the finite extent T/a of our gauge-field configurations and the use of anti-periodic boundary conditions for fermions in the time direction, we need to account for the “around-the-world effect” which enters with a different sign for $\langle AP \rangle$ than for the $\langle PP \rangle$ correlators. We therefore obtain \bar{R} in Eq. (4) from the combination $R(t/a; \tau/a^2) \cosh(M_{\text{PS}}(T/2 - t)) / \sinh(M_{\text{PS}}(T/2 - t))$. Since the pseudo-scalar mass M_{PS} can be measured very precisely (see Table S-II), this combination shows a long, flat plateau. We perform correlated fits to the plateaus from time slice 40 to 46 extracting the values of $\bar{R}(\tau/a^2)$ shown in the legend.

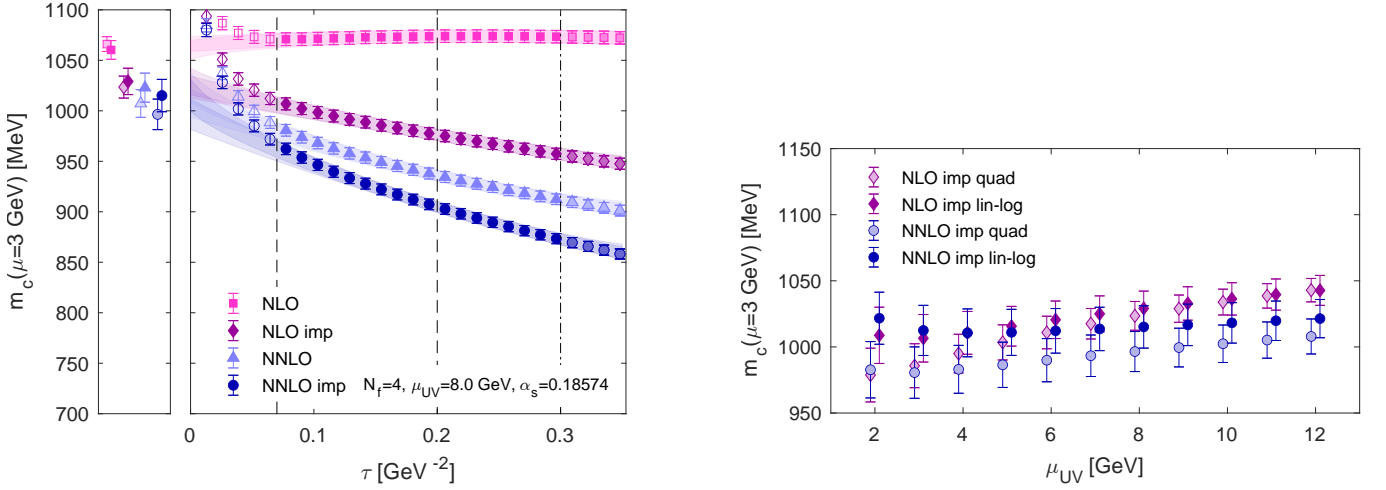


FIG. S-2. The large panel on the left illustrates extracting m_c using η_c correlators at the renormalization scale $\mu_{UV} = 8$ GeV, converted to $\mu = 3$ GeV using 4-loop $N_f = 4$ $\overline{\text{MS}}$ running. Pink squares and light blue triangles denote the NLO and NNLO values, respectively. Purple diamonds and dark blue circles show the corresponding RG improved NLO and NNLO values. The $\tau \rightarrow 0$ limit is taken in a $(\tau_{\min}, \tau_{\max})$ range as explained in the text. The shaded error bands show the maximal spread of quadratic or linear-log fits using the central values plus/minus their uncertainty. Only filled symbols enter the $\tau \rightarrow 0$ extrapolation. The small panel compares the final predictions using solid filled symbols for linear-log and shaded fillings for quadratic fits. Right: dependence of the result for m_c on the scale μ_{UV} .

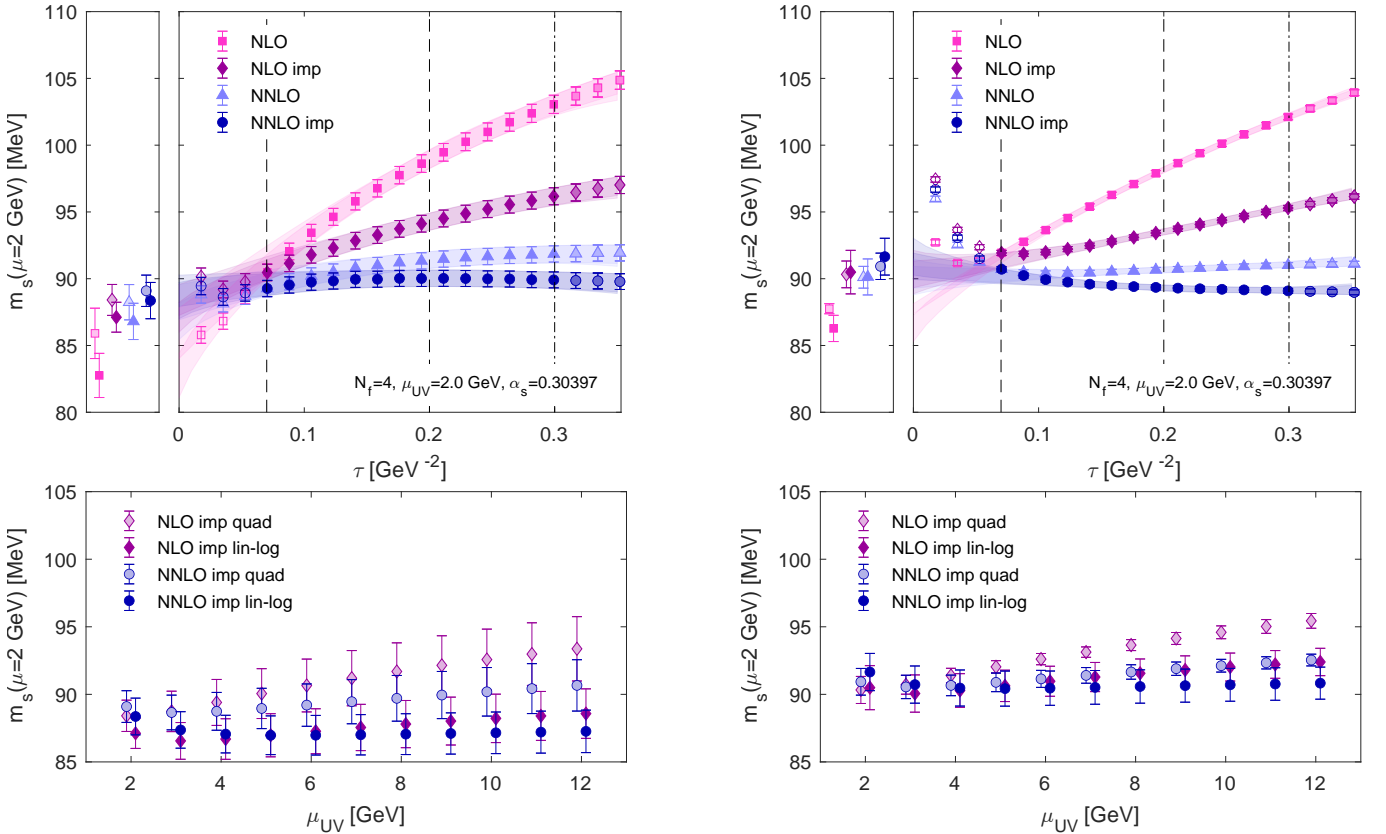


FIG. S-3. Extracting m_s using η_s correlators. Since the bare strange quark mass appears to be mistuned on the F1S ensemble (cf. Table S-II), we only analyze coarse and medium ensembles. Therefore we consider two continuum limits. The data on the left are obtained using an ansatz linear in a^2 , while data on the right result from fitting to a constant. Both continuum limits have good p -values and we quote the spread at $\mu = 2$ GeV as final result. The top row shows the $\tau \rightarrow 0$ extrapolation, the bottom row the μ_{UV} dependence. For further details see the description of Fig. S-2 above.